Journal of Alloys and Compounds, Volume 837, October 2020, Article number 155058
DOI:10.1016/j.jallcom.2020.155058

Hybrid Flash-SPS of $TiNiCu_{0.05}Sn$ with reduced thermal conductivity

Francesco Gucci [a,b] , Theo Graves Saunders [a]*, Bhuvanesh Srinivasan [c,d], François Cheviré[c], Daniella A. Ferluccio [e], Jan-Willem G. Bos [e], Michael J. Reece [a]

[a] School of Engineering and Material Science, Nanoforce Technology Limited, Queen Mary University of London, London E1 4NS, UK

[b] Department of Manufacturing and Materials, Cranfield University, Cranfield, Bedfordshire, MK43 0AL, UK

[c] University of Rennes, CNRS, ISCR – UMR 6226, F-35000 Rennes, France

[d] CNRS-Saint Gobain-NIMS, UMI 3629, Laboratory for Innovative Key Materials and Structures (LINK), National Institute for Materials Science, Tsukuba, 305-0044, Japan

[e] Institute of Chemical Sciences and Centre for Advanced Energy Storage and Recovery, School of Engineering and Physical Sciences, Heriot-Watt University, Edinburgh, UK

Abstract

$TiNiCu_{0.05}Sn$ was sintered using Spark Plasma Sintering (SPS) and a new derivative processing method, hybrid Flash-SPS (hFSPS). The high heating rate achieved (7700 °C/min) produced almost single-phase samples with high density. The sample sintered at 1040 °C showed a higher power factor and a lower thermal conductivity than the SPS sample, resulting in a higher ZT at 350 °C (0.44 vs 0.35).

Thermoelectric materials have received increased interest from the scientific community in recent years as they can be used to recover energy from waste heat. Their ability to produce electrical energy without moving parts makes them of great interest for many applications, as this can increase reliability and reduce maintenance costs. Their efficiency is linked to the dimensionless figure of merit $ZT = \sigma S^2 T/k$, where σ is the electrical conductivity, S is the Seebeck coefficient, T is the absolute temperature and k is the total thermal conductivity. ZT is used to compare the overall performance, while σS^2 (referred as Power Factor) is used to compare the power output of different materials [1].

Many materials with good potential thermoelectric properties have been identified, and half-Heusler (HH) alloys (based on TiNiSn) are suitable for intermediate-temperature applications (300-500°C). They generally possess a high power factor but also a high thermal conductivity, which limits their figure of merit [2]. Several strategies to lower thermal conductivity can be used, such as alloying, microstructure engineering and lattice disorder [3-5]. The thermal conductivity has two main components: the electronic contribution, related to the movement of electrons, and the lattice

contribution, related to the movement of phonons with a spectrum of wavelengths. The electronic contribution is linked to electrical conductivity through the Wiedemann-Franz law (direct proportionality) and cannot be significantly reduced without affecting electrical conductivity and therefore the Seebeck coefficient (lowering ZT). However, lattice thermal conductivity can be lowered by increasing the scattering of phonons. A phonon can be scattered by microstructural features having the same length scale, such as substitutional defects, vacancies or grain boundaries. Since phonons have different wavelengths, the best results can be achieved by producing microstructure having defects at different length scales [6].

The best figure of merit reported for an n-type half-Heusler was obtained by Sakurada et al.[7] for Sb-doped $Hf_{0.25}Zr_{0.25}Ti_{0.5}NiSn$ produced by solid-state reaction and hot pressing; the ZT was 1.5 at 700 K. Populoh et al. [8] produced $Ti_{0.37}Zr_{0.37}Hf_{0.26}NiSn$ by arc melting and annealing, obtaining a lower ZT of 1 at 750 K. Rogl et al.[9] achieved the same ZT as in Sakurada`s work for the same composition but at 823 K, and also investigated replacing Hf with V and Nb, and achieved a ZT of 1.2 and 1.1 respectively at 823 K. The replacement of Hf in HH alloys is of interest because of its high price, stimulating research to look developing materials using inexpensive elements. Downie et al.[10] found that Cu is a beneficial addition for increasing the power factor of HH alloys, which tends to replace Ni in the tetrahedral site occupancy (4*d*) but also produce some nano-segregated Ni and Cu phases, thus shifting the nominal composition to a Ni-richer one. The Cu presence induce an increase of the electrical conductivity acting as a good electron donor providing a significant reduction of resistivity and increase of power factor. The Cu content was further optimized by Barczak et al. [11], who found the optimum composition was $TiNiCu_{0.05}Sn$ and measured a peak ZT of about 0.6 at 723 K. It was also observed that the nominal composition of the HH compound was not homogeneous but when the Cu amount was below 0.1 it was fully allocated within the HH matrix. They also showed that processing has some influence on the lattice parameter, increasing the amount of dopant tended to increase the lattice parameter after synthesis, but after hot pressing the same powder the lattice parameter actually reduced. This implies that processing will affect how the dopant is integrated into the lattice.

As well as doping and composition, the microstructure of HH's is important to achieve good thermoelectric performance. Casting and sintering are the most common ways to control microstructure, with the most typical sintering techniques for thermoelectrics being hot-pressing and Spark Plasma Sintering (SPS). A new sintering method "flash sintering" has gained interest in the ceramic community [12]. Flash sintering exploits thermal runaway to produce fast heating (> 5000 °C/min) of small samples (< 1 cm^3 [12]). Flash sintering has mostly been investigated for relatively high electrical resistivity materials, which required a preheating stage for the samples to

become sufficiently electrically conductive. The method is capable of reducing sintering temperature [13], inducing atom migration [14] and the formation of second phases at grain boundaries [15].

Flash SPS (FSPS) is a derivative method that uses a SPS device to achieve high heating rates (> 5000 °C /s), it can also be used on large volume samples (> 1 cm^3 [12]) and to sinter relatively electrically conductive materials without any preheating. Initially FSPS was used for high temperature ceramics such as ZrB_2 [16], SiC [17], Yttria stabilized Zirconia [18], and hard magnetic materials Nd-Fe-B [19]. It has also been used for some thermoelectric materials, such as Magnesium Silicide-Stannide [20] and Titanium suboxides [21] with promising results. FSPS is a dieless configuration of SPS where the current is forced to pass through a pre-densified (samples must be pre-densified to support the minimum pressure applied by the SPS) sample and graphite punches. The electrical conditions are set to obtain the required sintering temperature and microstructure.

A limitation of the FSPS technique is that the samples need to be pre-sintered to achieve a minimum strength and the unconstrained deformation of the samples during high temperature sintering. To overcome this we have developed a hybrid of FSPS (hFSPS) involving the use of a thin conductive metal die [22] that allows powders to be directly flash sintered. In this work we have applied hybrid FSPS to evaluate the effect of rapid heating/sintering on a half-Heusler thermoelectric and compared it to conventional SPS.

$TiNiCu_{0.05}Sn$ powders were prepared using standard solid-state methods, as described by Barczak et al [11]. A SPS furnace (FCT HPD 25; FCT Systeme GmbH, Rauenstein, Germany) was used to sinter the powders. The conventional SPS setup used 15 mm diameter graphite punches and graphite die (10 mm wall thickness). The die had a hole drilled up to 3 mm from the surface to allow a thermocouple to measure the temperature. A single layer of graphite foil was used between the punches and the wall of the die to help with sample removal. Samples were sintered at 850 °C and 80 MPa (heating rate 100 °C/min, dwell time 12 min) under a vacuum of 3.5 Pa. A simple schematic of the temperature profiles is shown in Fig 1. The hFSPS setup used a 15 mm inside diameter stainless steel die (wall thickness 4 mm), with solid graphite punches with a hole drilled at 3 mm from the surface. A thermocouple was used for each punch to measure the temperature as well as any temperature gradients present. Stainless steel grade 304 was chosen for the Hybrid FSPS die as it has a good yield strength at high temperature (more than 200 MPa at 750 °C). While the sintering temperature of the half-Heusler exceeded 750 °C, this was not a problem as modeling and experience showed that the die was always at a much lower temperature than the sample and survived multiple uses. A pressure of 80 MPa was used to aid densification. To reduce the risk of overheating the

samples, they were initially preheated to 400 °C with a slow SPS heating profile 100 °C /min) and held for 30 s to normalize the temperature. A flash power pulse was then applied to reach the sintering temperature. The temperatures achieved were 980 °C (hFSPS-980, heating rate 7000 °C/min) and 1040 °C (hFSPS-1040, heating rate 7700 °C/min).

The density of the sintered samples was measured using the Archimedean method, electrical properties were measured using a Linseis LSR-3 with Pt thermocouples and electrodes. Thermal diffusivity was measured using the laser flash method in flowing Ar atmosphere using a Netzch LFA-457. The specific heat capacity of the samples was calculated using the Petit-Dulong equation as it has been proven to provide an accurate approximation, in particular above 500 K (less than 1% error) [11]. The microstructures of the samples were observed on fracture surfaces using a scanning electron microscope (SEM, FEI Inspect TM-F). XRD measurements were performed on powders and sintered samples using XRD (X'Pert PRO-PANalytical (Cu K-$L_{2,3}$ radiation, λ = 1.5418 Å, PIXcel 1D detector) to determine the phase contents. Rietveld refinement was performed using GSAS2 [23]. The lattice thermal conductivity was calculated as the difference between the total thermal conductivity and the electronic contribution. The electronic contribution to the thermal conductivity was calculated as $L\sigma T$ where L is the Lorenz number [24], σ is the electrical conductivity and T is the absolute temperature. The Lorentz number value used for the calculation of lattice contribution has been calculated using $L=1.5+\exp[-|S|116]$, as discussed by Kim et al.[24], the equation was proved to be a more reliable approximation than the constant value of 2.44×10^{-8} $W\Omega K^{-2}$ (see supporting information S1).

The XRD data (Fig 2) show that the starting powder was nearly single phase TiNiSn with minor traces of unreacted Sn which did not fully react even during sintering. This is surprising as the synthesis time of the powder was rather long (more than two weeks) [10]. The Sn peak remained clearly visible in the hFSPS-1040 sample, but the Sn peaks were difficult to detect in the SPS and hFSPS-980 samples. The presence of free Sn could induce some compositional variation within the grains, but such a variation would be very difficult to identify [10, 11]. Lattice parameters (Tab 1) were comparable to literature samples [11], thus confirming nominal composition, and processing had no significant effect on Cu content. Because of ultrafast heating and short processing time during hFSPS, there is not sufficient time for the sample to recrystallize and the dopants may not be evenly distributed and might have moved from their lattice positions, thus resulting in slight changes in their crystal structure. This reflects in the minimal changes in their lattice parameters, depending on the type and temperature of sintering.

The SPS sample also appeared to have traces of a full-Heusler phase, probably $TiNi_2Sn$, but no obvious composition contrast was observed in the backscattered SEM images (Fig 3-d). The thermo-electric transport properties are also probably influenced by the presence of impurities, in particular the Sn inclusion in hFSPS-1040 could have increased its electrical conductivity, as they are metallic, and provided additional interfaces for the scattering of phonons. The presence of full-Heusler phase ($TiNi_2Sn$) in SPS might be the reason for its higher resistivity, as secondary phases are generally known to increase resistivity.

The final density of all the samples was quite similar, the SPS and hFSPS-1040 samples were both 92.5% of the theoretical density, while the hFSPS-980 sample only reached 90% density. The fact that all the samples had similar densities provided a good opportunity to compare the different processing techniques, as only the thermoelectric properties and microstructure differed. While the samples were not fully dense porosity is not necessarily an obstacle to good thermoelectric performance and is sometimes induced intentionally to improve properties[25].

The starting powders consisted of mostly large agglomerates (about 100 μm) of smaller particles (about 5 μm), (S2). EDS analysis of the particles that appeared as a darker phase in backscattered imaging (S3) suggested that they were TiO_2 (S4). The presence of the oxide was not detectable in the XRD data. Traces of oxides were identified in all the samples, since they are unlikely to be reduced during the sintering, and could be the reason for the incomplete densification of the samples, as oxides are obstacles to sintering [26].

Images of the fracture surfaces showed some difference in the microstructures of the samples (Fig 3). The grain size (Fig 3-a) of the SPS sample was larger than the particle size of the starting powder because of the relatively slow heating rate used during sintering, allowing plenty of time for grain growth. The SPS grain size ranged from 10 to more than 20 μm. The surface appeared to be porous and rough, and the fracture path followed the grain boundaries. This implied weak bonding between the grains, which might have influenced the electrical conductivity of the samples. There was a trend between surface roughness/intergranular failure and electrical resistivity (Fig 4-a). The microstructure of the SPS samples showed large variations in grain size, clearly visible (Fig 3-a). Backscattered images of these regions (Fig 3-d) showed the presence of a brighter phase, probably the free-Sn (circled region). identified in the XRD data.

The hFSPS-980 sample had a similar fracture surface to the SPS sample with evidence of weak inter-grain bonding and appreciable porosity (Fig 3-b). High magnification backscattered images of the hFSPS-980 sample (Fig 3-e) showed the presence of a brighter phases (like the Sn-rich phases in the SPS sample) and grains with abnormal growth (large grains above 10 µm and small grains below 5 µm). Such mesoscale structuring is rather similar to that observed for other flashed materials [27, 28] and can influence the thermal conductivity by panoscopic scattering of phonons over a wide range of wavelengths [6].

The hFSPS-1040 sample had a completely different fracture surface from the previous two samples (Fig 3-c), despite having the same density as the SPS sample. The relatively smooth fracture surface indicated a trans-granular fracture, which could be due to the higher strength or coherency of the grain boundaries, which would be expected to improve electrical conductivity [29] (Fig 4-a). While the grain size could only be seen in regions that had intergranular fracture, in those regions the average size was a mix of smaller grains of about 5 µm and larger grains (> 20 µm, Fig 3-f) as well as submicron porosity. This mix of large and small grains with porosity was expected to reduce thermal conductivity because of multi-scale scattering effects. High magnification backscattered images (Fig 4-f) did not show any bright regions rich in Sn as seen in the other samples, which was surprising as Sn was visible in XRD of the sample (Fig 2).

The electrical properties of all the samples are shown in Fig 4 (a-b-c). The electrical resistivity of the samples followed the same trend, with resistivity increasing steadily from 323K to 623K (Fig 4-a). The hFSPS-1040 sample had the lowest value (about 20% lower than SPS). The Seebeck coefficients, however, did not follow the typical relationship of samples, with higher resistivity having higher value. Instead the hFSPS-1040 samples had the lowest resistivity while having a Seebeck between the SPS and hFSPS-980 sample (Fig 4-a-b). The lower resistivity and relatively higher Seebeck coefficient of the hFSPS-1040 sample contributed to its relatively high-power factor (Fig 4-c). While the hybrid flash process produced samples with a higher power factor compared to SPS, the power factor of the hFSPS-1040 sample was lower than hot pressed materials reported in the literature (3400 mW/m*K vs 2400 mW/m*K at 350 °C) [11]. However, the thermal conductivity was reduced, particularly for the hFSPS-1040 sample (Fig 4-d), which had the lowest value (3.79 W/m*K at 350 °C) thanks to a reduced lattice contribution (Fig 4-e), while the materials reported in literature [11] had values of about 4.6 W/m*K. This indicated that the microstructure produced by flash sintering was the main contributor to the reduced thermal conductivity, since the hFSPS-1040 sample had the same density as the SPS sample. It is difficult to pinpoint the exact mechanism responsible for these

improvements, but previous works suggest some degree of meso-structuring was beneficial [22, 27, 28], hFSPS could also provide a way to optimize the charge-carrier density and at the same time benefit from the decreased lattice thermal conductivity without significantly affecting the carrier mobility [27, 28]. The low thermal conductivity and the good power factor of the hFSPS-1040 sample allowed it to achieve a peak ZT of 0.44 at 350 °C (SPS only reached 0.35), comparable to the literature (about 0.46 at 350 °C) [11].

In this work we studied the effect of hFSPS processing of a half-Heusler and showed that hFSPS processing has the potential to reduce lattice thermal conductivity. The high heating rate used (7700 °C/min) and short processing time (5 min vs 32 min), significantly reduced both energy consumption and processing time. Despite the reduced processing time, a good density (92.5%) was achieved and the properties were comparable or higher than state of art sintering technologies (hot press and SPS) for similar compositions, with a peak figure of merit of 0.44 at 350 °C. Further work will be required to optimize the process (temperature, doping, powder size distribution) to achieve not only a reduction of thermal conductivity but also optimization of the electrical properties. One particularly interesting avenue to pursue would be investigating how the optimum doping concentration and associated charge carrier concentrations change due to rapid heating.

Acknowledgements

F.G. and B.S. were supported by European Community's Horizon 2020 Programme through a Marie Skłodowska-Curie Innovative Training Network [g.a. no. 642557, CoACH-ETN]; J-WGB would like to acknowledge the support of EPSRC grant EP/N01717X/1.

Figure 1 Schematic of the heating profile for: a) SPS; b) hFSPS-980; and c) hFSPS-1040

Figure 2 XRD patterns of all the samples and peak position of identified phases

Table 1 Refined lattice parameters for all samples

Figure 3 SEM secondary electron images of: a) SPS (overgrown grains circled); b) hFSPS-980; and c) hFSPS-1040. Backscattered electron images of: d) SPS; e) hFSPS-980; and f) hFSPS-1040 (brighter spots are circled when visible)

Figure 4 Properties of the samples: a) Electrical resistivity; b) Seebeck coefficient; c) Power factor; d) Thermal conductivity e); Lattice thermal conductivity; and f) Figure of merit. The key transport properties of $TiNiCu_{0.05}Sn$ are compared with the recent literature reports (ref 10, 11).

References

1. Rowe, D.M., *CRC Handbook of Thermoelectrics*. 1995.
2. Sootsman, J.R., D.Y. Chung, and M.G. Kanatzidis, *New and Old Concepts in Thermoelectric Materials.* Angewandte Chemie-International Edition, 2009. **48**(46): p. 8616-8639.
3. Alam, H. and S. Ramakrishna, *A review on the enhancement of figure of merit from bulk to nano-thermoelectric materials.* Nano Energy, 2013. **2**(2): p. 190-212.
4. Srinivasan, B., et al., *Enhancement in thermoelectric performance of n-type Pb-deficit Pb-Sb-Te alloys.* Journal of Alloys and Compounds, 2017. **729**: p. 198-202.
5. Srinivasan, B., et al., *Thermoelectric Properties of Highly-Crystallized Ge-Te-Se Glasses Doped with Cu/Bi.* Materials, 2017. **10**(4).
6. Zhao, L.D., V.P. Dravid, and M.G. Kanatzidis, *The panoscopic approach to high performance thermoelectrics.* Energy & Environmental Science, 2014. **7**(1): p. 251-268.
7. Sakurada, S. and N. Shutoh, *Effect of Ti substitution on the thermoelectric properties of (Zr,Hf)NiSn half-Heusler compounds.* Applied Physics Letters, 2005. **86**(8).
8. Populoh, S., et al., *High figure of merit in (Ti,Zr,Hf)NiSn half-Heusler alloys.* Scripta Materialia, 2012. **66**(12): p. 1073-1076.
9. Rogl, G., et al., *(V,Nb)-doped half Heusler alloys based on {Ti,Zr,Hf}NiSn with high ZT.* Acta Materialia, 2017. **131**: p. 336-348.
10. Downie, R.A., et al., *Metal Distributions, Efficient n-Type Doping, and Evidence for in-Gap States in TiNiMySn (M = Co, Ni, Cu) half-Heusler Nanocomposites.* Chemistry of Materials, 2015. **27**(7): p. 2449-2459.
11. Barczak, S.A., et al., *Grain-by-Grain Compositional Variations and Interstitial Metals—A New Route toward Achieving High Performance in Half-Heusler Thermoelectrics.* ACS Applied Materials & Interfaces, 2018. **10**(5): p. 4786-4793.
12. Yu, M., et al., *Review of flash sintering: materials, mechanisms and modelling.* Advances in Applied Ceramics, 2017. **116**(1): p. 24-60.
13. Cologna, M., B. Rashkova, and R. Raj, *Flash Sintering of Nanograin Zirconia in < 5 s at 850 degrees C.* Journal of the American Ceramic Society, 2010. **93**(11): p. 3556-3559.
14. Biesuz, M., et al., *Investigation of Electrochemical, Optical and Thermal Effects during Flash Sintering of 8YSZ.* Materials, 2018. **11**(7): p. 1214.
15. Uehashi, A., et al., *Formation of secondary phase at grain boundary of flash-sintered BaTiO<inf>3</inf>.* Microscopy, 2014. **63**(suppl_1): p. i19-i20.
16. Grasso, S., et al., *Flash Spark Plasma Sintering (FSPS) of Pure ZrB2.* Journal of the American Ceramic Society, 2014. **97**(8): p. 2405-2408.
17. Grasso, S., et al., *Flash Spark Plasma Sintering (FSPS) of and SiC.* Journal of the American Ceramic Society, 2016. **99**(5): p. 1534-1543.
18. Vasylkiv, O., et al., *Flash spark plasma sintering of ultrafine yttria-stabilized zirconia ceramics.* Scripta Materialia, 2016. **121**: p. 32-36.
19. Castle, E., et al., *Rapid sintering of anisotropic, nanograined Nd-Fe-B by flash-spark plasma sintering.* Journal of Magnetism and Magnetic Materials, 2016. **417**: p. 279-283.
20. Du, B.L., et al., *Flash spark plasma sintering of magnesium silicide stannide with improved thermoelectric properties.* Journal of Materials Chemistry C, 2017. **5**(6): p. 1514-1521.
21. Yu, M., et al., *Magnéli phase titanium suboxides by Flash Spark Plasma Sintering.* Scripta Materialia, 2018. **146**: p. 241-245.
22. Gucci, F., T.G. Saunders, and M.J. Reece, *In-situ synthesis of n-type unfilled skutterudite with reduced thermal conductivity by hybrid flash-spark plasma sintering.* Scripta Materialia, 2018. **157**: p. 58-61.

23. Toby, B.H. and R.B. Von Dreele, *GSAS-II: the genesis of a modern open-source all purpose crystallography software package.* Journal of Applied Crystallography, 2013. **46**(2): p. 544-549.
24. Kim, H.-S., et al., *Characterization of Lorenz number with Seebeck coefficient measurement.* APL Materials 2015. **3**(4): p. 041506.
25. Chen, X., et al., *Porosity-mediated high-performance thermoelectric Materials.* arXiv preprint arXiv:1810.03356, 2018.
26. Munir, Z.A., *Surface Oxides and Sintering of Metals.* Powder Metallurgy, 1981. **24**(4): p. 177-180.
27. Srinivasan, B., et al., *Effect of the Processing Route on the Thermoelectric Performance of Nanostructured CuPb18SbTe20.* Inorganic Chemistry, 2018. **57**(20): p. 12976-12986.
28. Srinivasan, B., et al., *Realizing a stable high thermoelectric zT ∼2 over a broad temperature range in Ge1−x−yGaxSbyTe via band engineering and hybrid flash-SPS processing.* Inorganic Chemistry Frontiers, 2019. **6**(1): p. 63-73.
29. Lu, K., L. Lu, and S. Suresh, *Strengthening Materials by Engineering Coherent Internal Boundaries at the Nanoscale.* 2009. **324**(5925): p. 349-352.

Table

Sample	Lattice parameter a (Å)
Powder	5.9399(1)
SPS	5.9415(4)
hFSPS-980	5.9412(3)
hFSPS-1040	5.9430(1)

Figure 1

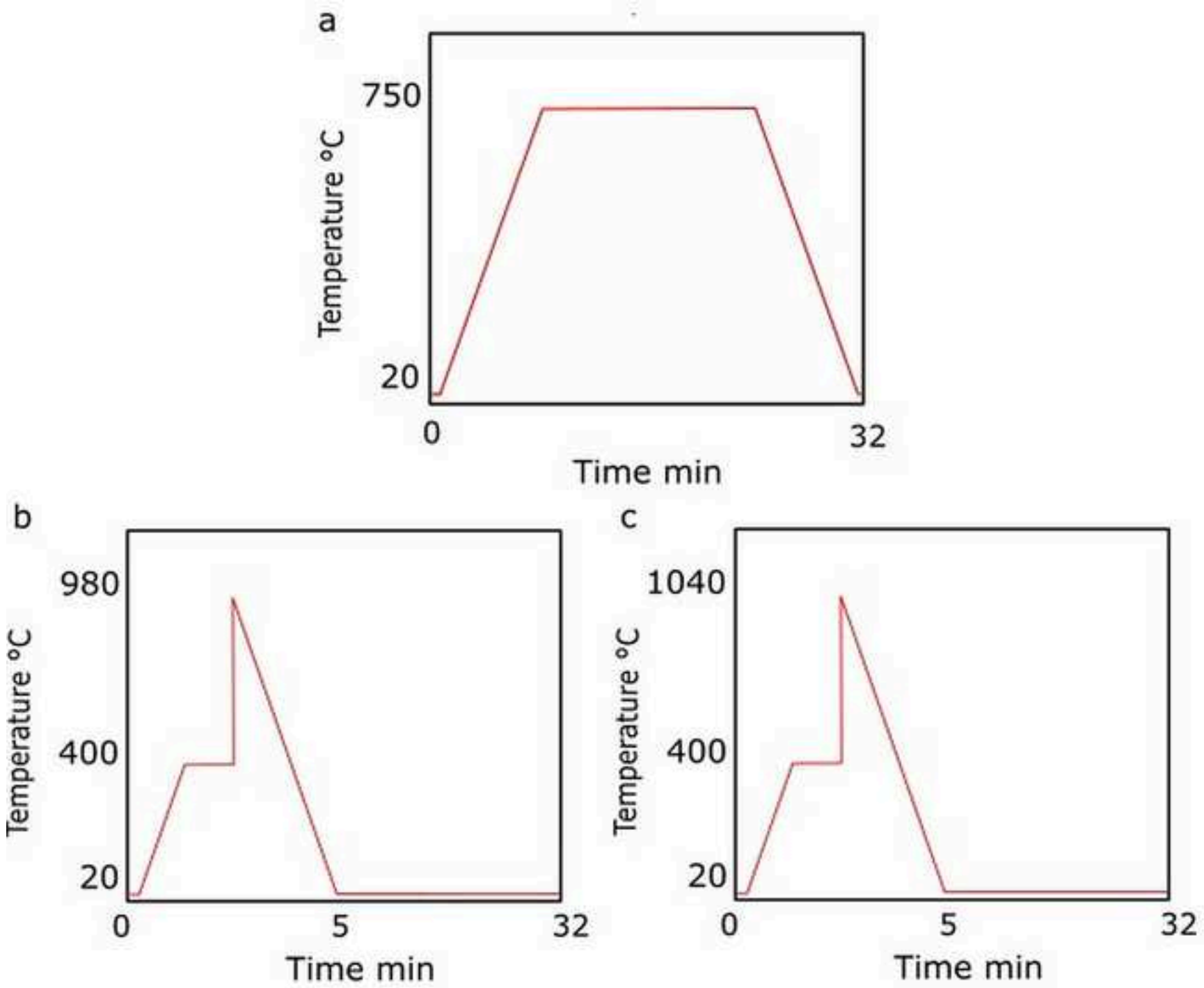
a
750
20
Temperature °C
0
32
Time min
b
980
400
20
Temperature °C
0
5
32
Time min
c
1040
400
20
Temperature °C
0
5
32
Time min

Figure 2

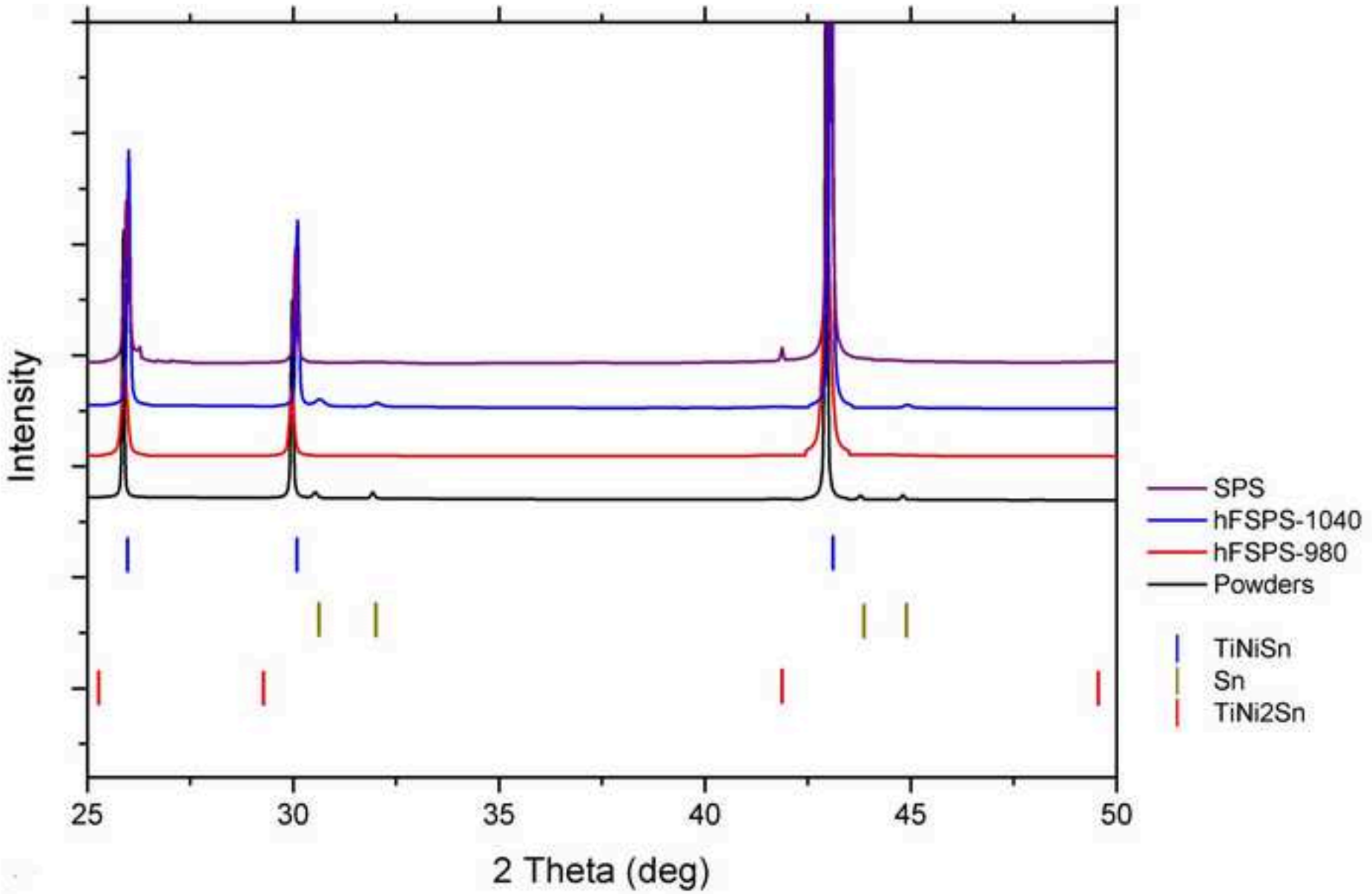
Intensity
25
30
35
40
45
50
2 Theta (deg)
SPS
hFSPS-1040
hFSPS-980
Powders
TiNiSn
Sn
TiNi2Sn

Figure 3

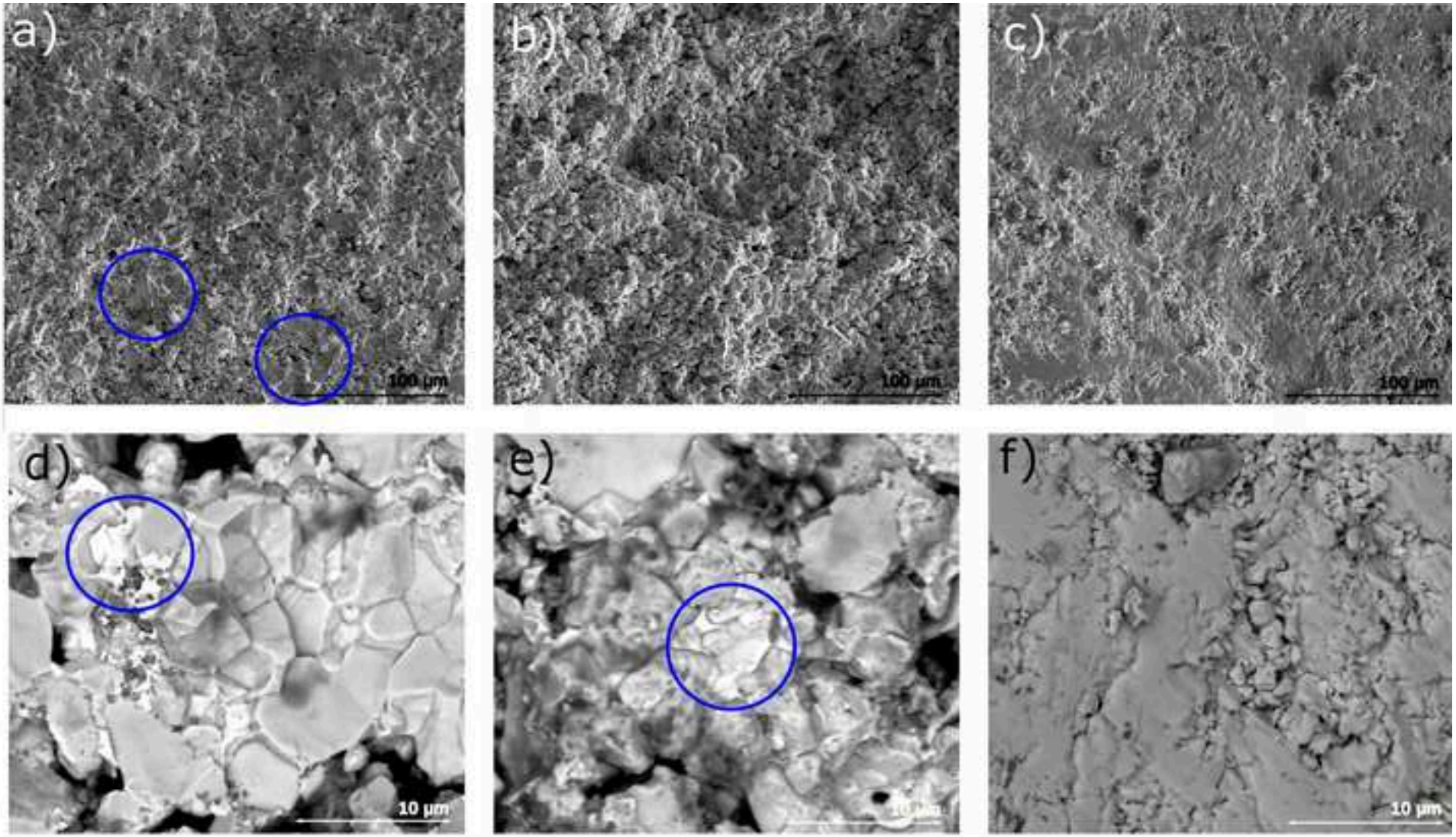

Figure 4

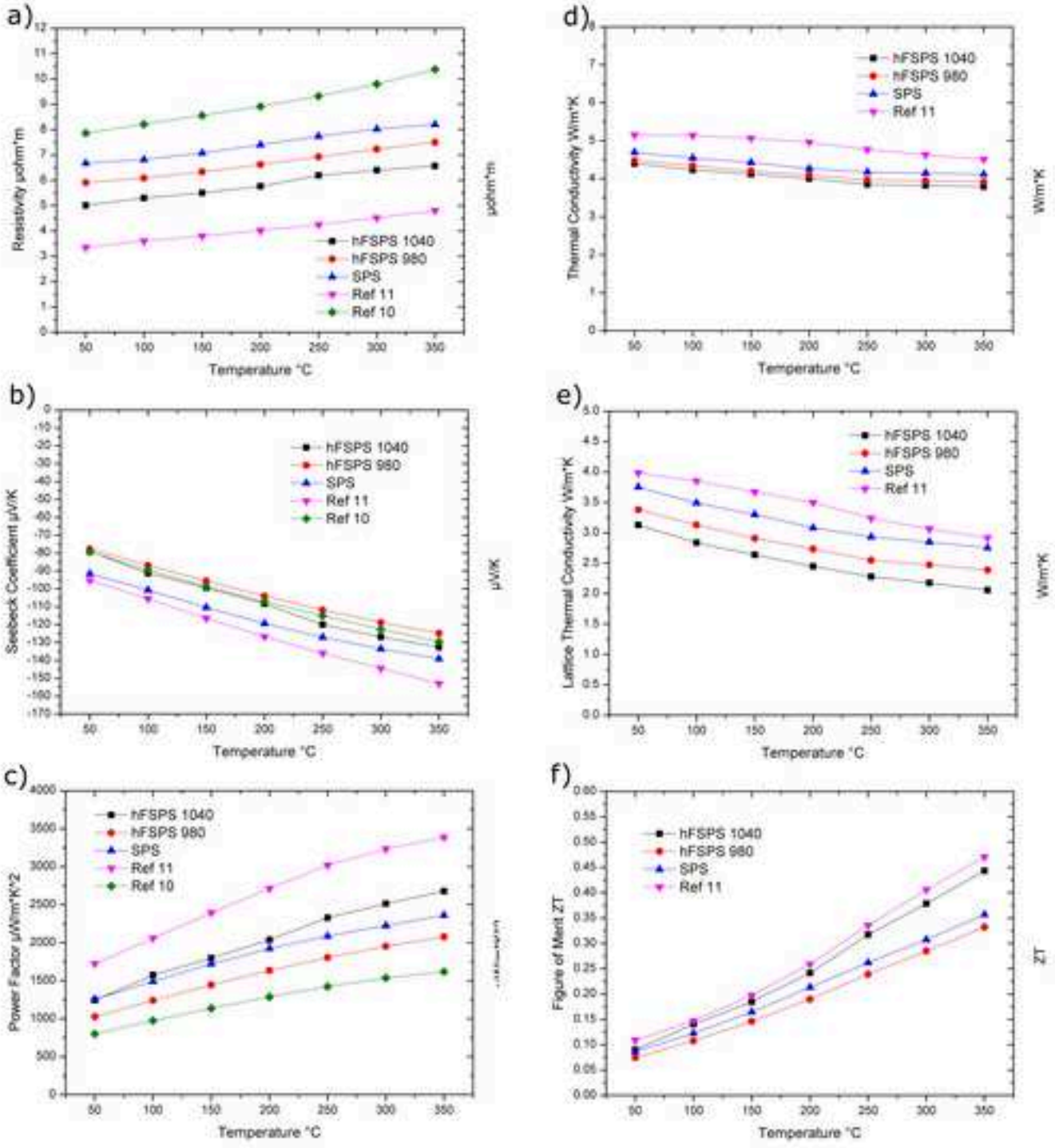
a)
Resistivity µohm*m
µohm*m
Temperature °C
hFSPS 1040
hFSPS 980
SPS
Ref 11
Ref 10
b)
Seebeck Coefficient µV/K
µV/K
Temperature °C
hFSPS 1040
hFSPS 980
SPS
Ref 11
Ref 10
c)
Power Factor µW/m*K^2
Temperature °C
hFSPS 1040
hFSPS 980
SPS
Ref 11
Ref 10
d)
Thermal Conductivity W/m*K
W/m*K
Temperature °C
hFSPS 1040
hFSPS 980
SPS
Ref 11
e)
Lattice Thermal Conductivity W/m*K
W/m*K
Temperature °C
hFSPS 1040
hFSPS 980
SPS
Ref 11
f)
Figure of Merit ZT
ZT
Temperature °C
hFSPS 1040
hFSPS 980
SPS
Ref 11

Hybrid Flash-SPS of TiNiCu0.05Sn with reduced thermal conductivity

Gucci, Francesco

2020-04-06

Gucci F, Saunders TG, Srinivasan B, et al., (2020) Hybrid flash-SPS of TiNiCu0.05Sn with reduced thermal conductivity. Journal of Alloys and Compounds, Volume 837, October 2020, Article number 155058

https://doi.org/10.1016/j.jallcom.2020.155058